Springer

Journal of
Mechanical
Science and
Technology

Journal of Mechanical Science and Technology 22 (2008) 1202~1212

www.springerlink.com/content/1738-494x

Natural convection between concentric spheres in electromagnetic fields

Chung-Hyo Jung[1,*] and Takahiko Tanahashi[2]

[1]*Samsung Electronics CO., LTD., 416 Maetan-3Dong, Yeongtong-Gu, Suwon-City, Gyeonggi-Do, Korea*
[2]*Faculty of Science and Technology, Keio University, 3-14-1, Hiyoshi, Kouhoku-Ku, Yokohama, 223-8522, Japan*

(Manuscript Received September 28, 2007; Revised March 3, 2008; Accepted March 23, 2008)

Abstract

This study performs numerical analyses for two different working fluids. One is an analysis of natural convection using a model with air that is compared with the results of applied experiments. Then, it can be used to investigate the pattern of natural convection in concentric spheres. The other is an investigation for the relationship between velocity field, electromagnetic field, and temperature field in a model with molten metal. The subject of the analysis model is the natural convection between two concentric spherical shells. In particular, a process where induced magnetic fields intensify the imposed magnetic field can be called a dynamo process. This study uses a modified *B* method in order to investigate the role of this induced magnetic field. This method is also compared to a Φ method that only considers imposed magnetic fields. In addition, this study examines the relationship between the velocity field and the electromagnetic field for the velocity field through applying Coriolis forces.

Keywords: Numerical analysis; Natural convection; GSMAC-FEM; MHD; Φ method; *B* method; Coriolis force; Lorentz force; Two concentric spheres; Induced magnetic field

1. Introduction

Natural convection can be observed in huge scaled natural phenomena that are represented as the air of the earth, the convection of the ocean, and the convection of the outer core and mantle inside the earth and that can be extended to certain applications, such as the design of atomic plants, light fixtures, and other various engineering fields. An example of natural convection can be implemented by using a space with two concentric spheres in which the space formed by the inner and the outer space is filled by a certain fluid and a temperature gradient is applied from the surface of the inner sphere to the outer sphere. This phenomenon is an easily understood natural phenomenon that has been studied for a long time ago as an issue of engineering natural convection. In particular, because the convection of molten metal, such as mercury and sodium, includes flow fields, electromagnetic fields, and temperature fields, it has been regarded as a core of energy science.

In the case of the two concentric spheres, some studies reported detailed investigations on the flow of fluid and heat, and temperature distribution in such spheres when the working fluid was configured as air. Also, there are some results of the numerical analysis for the low *Ra* number (less than 10^5). In addition, the types of velocity and temperature fields are already investigated for the condition of $Ra<10^5$ because the results of this analysis nicely agree with the results of their experiments. However, there are few numerical analyses for the high *Ra* number (more than 10^5). Thus, this study performs a numerical analysis for the high *Ra* number in order to guarantee the reliability of applied numerical models. However, it is difficult to find certain experiments or numerical analyses including electromagnetic effects in the case of a working fluid that is given by molten metal. In previous studies, the convective controllable effect of the flow

*Corresponding author. Tel.: +82 31 277 7178, Fax.: +82 31 277 7733
E-mail address: chunghyo.jung@samsing.com
DOI 10.1007/s12206-008-0314-z

field was proved by using a Φ method as a solution of electromagnetic fields. However, the Φ method does not consider the induced magnetic field because it can be used as the induced magnetic field is negligible due to the fact that the imposed magnetic field applied in the Φ method shows a very low level compared to that of the imposed magnetic field.

This study examines the relationship between velocity, electromagnetic, and temperature fields by considering the induced magnetic field (for a magnetic *Re* number of $Rem \geqq 1$). In particular, a process where induced magnetic fields intensify the imposed magnetic field can be called a dynamo process. Although several researchers have analyzed the convective controllable effect using a *B* method, they failed in the implementation of the role of the dynamo. This study investigates the role of the dynamo by introducing a modified *B* method in the analysis of electromagnetic fields in order to verify the role of the induced magnetic field that intensifies the imposed magnetic field. In addition, this study considers the relationship between the velocity field and the electromagnetic field for the velocity field through applying Coriolis forces.

2. Numerical method

2.1 Basic equations

Governing equations can be obtained from the equation that forms velocity, electromagnetic, and temperature fields. The equation of the velocity field can be obtained by using the Navier-Stokes equation and the equation of continuity in which the Navier-Stokes equation uses an equation that is represented as a rotational form. The dimensionless can be performed using the *Ek* number (viscosity term/Coriolis term). In addition, the governing equation can be simplified by the following assumptions.

(a) An electromagnetic fluid is a type of conductive Newtonian fluid.

(b) The fluid is laminar and incompressible.

(c) In Eq. (2), the density noted in the buoyancy force term depends on the thermal expansion coefficient (β) and applied temperature.

(d) The external forces applied to the electromagnetic fluid are the buoyancy force, Coriolis force, and Lorentz force.

(e) Displacement electric currents are negligible.

(f) The electromagnetic fluid shows neutrality and non-polarity electrically.

(g) Temperature dependencies in material properties are negligible.

$$\nabla \cdot \boldsymbol{v} = 0 \tag{1}$$

$$\frac{\partial \boldsymbol{v}}{\partial t} = \nabla H + \boldsymbol{v} \times \boldsymbol{\omega} + Pr\,[\nabla^2 \boldsymbol{v} + Ta^{1/2} \boldsymbol{v} \times \hat{\boldsymbol{k}} + Ha^2 \boldsymbol{j} \times \boldsymbol{B} + RaT\,\hat{\boldsymbol{g}}] \tag{2}$$

where $\boldsymbol{v}$, H, $\boldsymbol{\omega}$, $\boldsymbol{k}$, $\boldsymbol{j}$, $\boldsymbol{B}$, T, and $\hat{\boldsymbol{g}}$ represent the velocity vector, Bernoulli function, vorticity vector, unit vector along the rotational axis, current density vector, magnetic flux density vector, temperature, and unit vector along the gravity, respectively. Also, the applied dimensionless numbers, *Pr*, *Ta*, *Ek*, *Ha*, and *Ra*, demonstrate the Prandtl number, Taylor number, Ekman number, Hartmann number, and Rayleigh number, respectively. They can be determined as follows:

$$Pr = \frac{\nu}{\alpha},\ Ta = \left(\frac{2\Omega d^2}{\nu}\right)^2,\ Ek = \frac{\nu}{2\Omega d^2},\quad Ha = \sqrt{\frac{\sigma}{\rho\nu}}\,Bd,\ Ra = \frac{\beta g d^3 \Delta T}{\alpha\nu} \tag{3}$$

In Eq. (3), it shows a formula of $Ra=Gr\cdot Pr$, where Ω, d, and ΔT represent the angular velocity, gap width between spheres (r_o-r_i), and temperature difference between the outer and the inner spheres, respectively. Also, elements ν, α, g, β, σ, and ρ show the of kinematic viscosity, thermal diffusivity, gravitational acceleration, thermal expansion coefficient, electric conductivity, and mass density of the fluid, respectively.

The equation of electromagnetic fields can be classified as Φ and *B* methods according to the manner of solution. The Φ method can be obtained by using the conservative law of currents and Ohm's law. In addition, the *B* method can be formed by using Gauss' law and the Maxwell equation. The equations used in the Φ method that only processes direct current magnetic fields are determined as follows:

$$\nabla \cdot \boldsymbol{j} = 0 \tag{4}$$

$$\boldsymbol{j} = -\nabla \Phi + (\boldsymbol{v} \times \boldsymbol{B}_0) \tag{5}$$

where Φ is the electric scalar potential. The equations used in the *B* method that deals with both imposed and induced magnetic fields are expressed as follows:

$$\nabla \cdot \boldsymbol{B}' = 0 \tag{6}$$

$$\frac{\partial \mathbf{B}'}{\partial t} = -\nabla R + (\mathbf{B}_0 \bullet \nabla)\mathbf{v} - (\mathbf{v} \bullet \nabla)\mathbf{B}' + \frac{1}{Rem}\nabla^2 \mathbf{B}' \tag{7}$$

$$\boldsymbol{j} = \frac{1}{Rem} \nabla \times \boldsymbol{B}' \tag{8}$$

where R and Rem are the dimensionless cross helicity (R= ($\nabla \cdot B$)/Rem) and the magnetic Reynolds number (Ud/ν_m), respectively. In the Navier-Stokes equation, the magnetic flux density vector, B, can be expressed as $B = B_0 + B'$ including the imposed magnetic field and the induced magnetic field. This approach that produces the vector, B, is called the modified B method.

In addition to the flow and electromagnetic field, the temperature field can be obtained from the energy equation. If the relation described by the Peclet number (Pe)=$Re \cdot Pr$=1 is used in the flow field with a high Ra number, the numerical analysis of the energy equation can be stably obtained. The Eckert number in the equation can be determined as $U/(C_p \Delta T)$.

$$\frac{\partial T}{\partial t} = -(\boldsymbol{v} \cdot \nabla) T + \nabla^2 T + PrHa^2 Ec \boldsymbol{j}^2 \tag{9}$$

2.2 Time marching algorithm

The discretization of velocity fields can be processed by using a GSMAC (Generalized Simplified Marker and Cell) method. The electromagnetic field in the B method is also discretized by using a simultaneous relaxation repetition method. Also, a forward Euler method can be used in temperature fields. In a way in the time marching algorithm for each physical field, the velocity field applies time processing with Eq. (2) for the function of H determined in a Bernoulli function implicitly and for other variables explicitly. Here, the velocity and Bernoulli function are to be modified in order to satisfy the incompressible condition at a time step of (n+1). The electromagnetic field used in the B method applies time processing with Eq. (7) for the vector, $\boldsymbol{v}$, and error function, R, implicitly and for the magnetic flux density vector, $\boldsymbol{B}$, explicitly, in which the magnetic flux density vector, $\boldsymbol{B}$, is to be modified to satisfy Gauss's law, Eq. (6) at a time step of (n+1). Also, the temperature field applies time processing with Eq. (9) for the velocity vector, $\boldsymbol{v}$, and current density vector, $\boldsymbol{j}$, implicitly and for the temperature, T, explicitly, in which a term of BTD is used to stabilize the solution for each physical field. In addition, the Galerkin method can be used to extract an element matrix equation. In the application of an interpolation function, an interpolation process is required for an eight-node isoparametric element for the elements of $\boldsymbol{v}$, $\boldsymbol{j}$, $\boldsymbol{B}$, and T and for the constant in the element for other variables. Here, the weighted functions, $\delta\boldsymbol{v}$, $\delta\boldsymbol{j}$, $\delta\boldsymbol{B}$, and δT, which become zero at a fixed boundary is used.

3. Numerical model

3.1 Analytical model

An analytical model is subject to the issue of the natural convection between two spherical shells. To generate such natural convection, it is necessary to configure the inner and outer spheres as a hot and cold state, respectively. The buoyancy force generated by the heat that is transferred from the inner sphere to the outer sphere becomes the motive force of natural convection. Fig.1 illustrates an analytical model. The gravitational force that is applied to fluids as a type of external force was configured as the direction of -Z. In the case of the fluid, which is configured as air, between shells, the diameters of the inner sphere were configured as 0.4 (Di/d=1.3), 0.6 (Di/d=3), and 0.8 (Di/d=8) to perform this analysis. Also, it was configured as 0.3 for molten metals. Whereas, Di and d represent the diameter and, r_o - r_i of the inner sphere, respectively.

3.2 Calculation area

In the case of the fluid, which is configured as air, in a calculation area, the mesh applied in the calculation was a type of hexahedron element and the total elements and nodes used in this calculation were determined as 384,000 and 393,682, respectively. Also, the minimum width of the applied mesh was 0.017 r_o. In the case of the molten metal, the generation of the

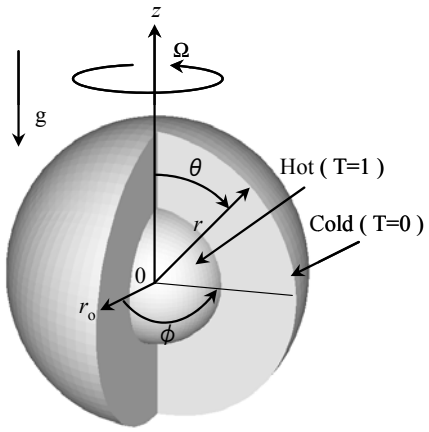

Fig. 1. Analytical model.

mesh was performed as a manner of unequal division based on Fan's numerical analysis. The mesh was generated to maintain the mesh width between the inner and the external side of the concentric sphere that shows a 1/3 times for the central mesh. The mesh used in this calculation was a type of hexahedron element and the total elements and nodes were determined as 48,000 and 550,442, respectively. Also, the minimum width of the applied mesh was 0.019 r_o.

3.3 Boundary condition

In Fig. 1, the boundary condition of the fluid velocity was configured as no slips at all wall surfaces. Also, in the case of the Φ method, the boundary condition of the current was configured as an insulation condition. In the *B* method, the boundary condition of the magnetic flux density was configured so that the normal component is to be determined as 0. The boundary condition of the temperature was determined as 1 and 0 for the external and internal side of the inner sphere, respectively. In addition, it was assumed that there are no heat transfers at the boundary between the internal side of the inner sphere and the external side of the outer sphere.

3.4 Numerical condition

In the case of the working fluid, which is determined as air, it was determined that there are no Coriolis forces. Here, the *Pr* number was determined as 0.71. Also, the *Ra* numbers were configured as 749,760, 229,330, and 5,964 for the radius ratios of 0.4, 0.6, and 0.8, respectively, in order to match it to the experimental results where the minimum calculation time (*dt*) was determined as 0.0002 for these conditions. In the solution of the Poisson equation, the element of ε (discrete equations: Eq. (1), (4), and (6)) was configured to satisfy the convergence condition for all elements through configuring it as 0.001 in which the iteration was determined up to 200 times. In addition, the calculation parameters applied in the Φ and *B* method that deal molten metals were configured as the same value except for the electromagnetic Reynolds number. In both methods, the *Pr*, *Ra*, and *Ha* numbers were configured as 0.25, 100, and 100, respectively. In the *B* method, the Coriolis force can be used as a type of external force in which the dimensionless numbers (*Ta* number) were configured as four different levels, such as 0, 10^2, 10^3, and 10^4. Also, the *Ec* number, convergence condition, and iteration were configured as 3.88×10^{-7}, 0.001, and 200. In both methods, the minimum calculation time, time increments (*dt*), was determined as 0.00002. Furthermore, the residual condition and iteration were determined as the same condition as the case that applied air.

3.5 Imposing magnetic field

It is necessary to apply electromagnetic fields under the condition where thermal convection is fully developed. The external electromagnetic field was applied along the direction of -*Z* and its scale was 1.

3.6 Magnetic Reynolds number

The magnetic Reynolds number has important meaning for the *B* method. As a size of laboratory scale, the magnetic Reynolds number shows less than 1. In a practical calculation of this number at room temperature, it is represented as $Rem=\mu\sigma Ud=0.0001$ (where, the representative length and representative velocity were determined as $d=0.01m$ and $U=0.01m/s$, respectively). However, the *B* method can be used as an effective method for $Rem \geqq 1$. In this study, the magnetic Reynolds number was applied by 1 in order to compare the Φ method with the *B* method.

4. Numerical results and discussion

4.1 Natural convection of air

Fig. 2 shows the results of the numerical analysis and Yin's visualization experiment applied in this study. The study of Yin's visualization was performed by using tobacco smoke and the behavior was recorded as pictures. Because the smoke is dispersed before the moment where the fluid is fully developed, the picture was produced at a condition of underdevelopment. As shown on the right side of Fig. 2(a), (b), and (c), there exist certain vortexes of the Crescent eddy flow and Kidney-shaped eddy flow. Fig. 2(b) and (c) show some distortions in a low velocity layer at the center of the vortex under the unsteady state. As shown in Fig. 2(b), however, certain vibrations occurred at the center as a radial shape and that were transferred from the center of the vortex to the inner sphere. It is difficult to express this phenomenon by a numerical analysis. A transient analysis is required to compensate the result. In addition, the results of the experiment presented in Fig. 2(c) dem-

onstrate a periodic contraction during the collapse of the center of the vortex. This contraction is well determined in the numerical analysis where the fluid velocity is not affected by the vortex at around the external wall of the inner sphere. Thus, it is evident that the fluid, which represents the Kidney-shaped eddy flow, includes complex motion.

Fig. 3 illustrates the flow pattern between two concentric sphere shells for the *Ra* number. Yin classified the convection patterns using the results of Bishop's experiment by comparing it with the results of his own experiment. It is possible to recognize that the flow becomes a type of unsteady flow according to the increase in the *Ra* number and radius ratio from the classification of such patterns. This analysis calculated the flow state of the unsteady region through applying a steady algorithm. Differences in the results between the experiment and its analysis as illustrated in Fig. 3 are due to the application of the steady flow algorithm in the calculation process instead of using the unsteady flow algorithm. It was verified that the region determined by a 0~18 of radius ratio and *Ra* number $\leqq 10^6$ can be calculated with the GSMAC-FEM. However, it is necessary to apply more advanced flow stabilization methods or unsteady algorithms over these conditions.

4.2 Natural convection of mercury under electromagnetic fields

By configuring a state model where the space between two concentric sphere shells is filled by molten metal, this model was analyzed to obtain a solution. Fig. 4 shows the results of the analysis of the velocity field under the condition that does not include electromagnetic fields. The conditions applied in this analysis were *Pr*=0.025, *Ra*=100, *Ta*=0, and *Ha*=0. Fig. 4 shows the velocity vector for the section at θ=90° and ϕ=90°. Whereas, the thermal convection showed certain development while it maintained a symmetric state at the dimensionless time of *t*=100. Because the applied metal, mercury, has a time dependency, however, it has been known that it is periodically vibrated according to the passage of time. Based on this idea, the region that represents such a time dependency was determined at *Ra* $\geqq$12,000. Thus, it is natural that there are no particular time dependencies in the mercury for the calculation of Ra=100. Next, this study considers the results of the calculation shown in Fig. 4 by applying imposed

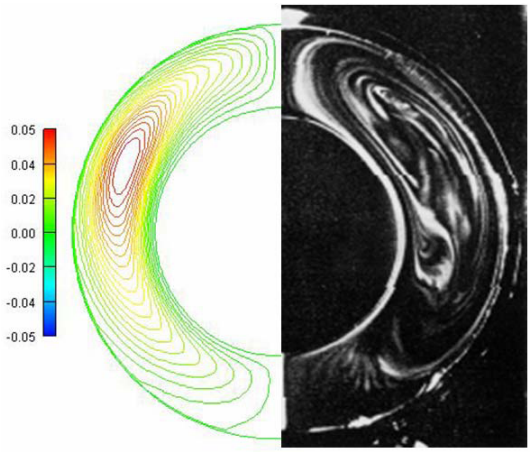

(a) Crescent eddy flow (*Di*/*d*=8, *Ra*=5,964)

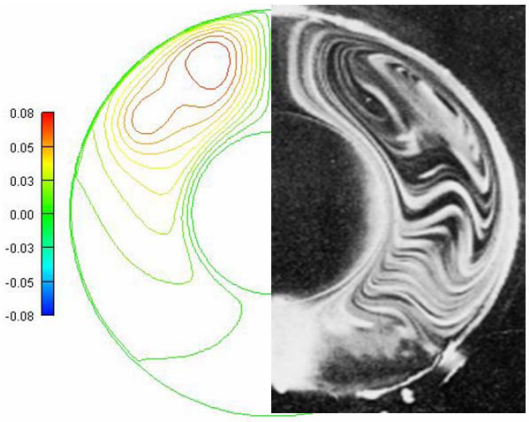

(b) Kidney-shaped eddy flow (*Di*/d=3, *Ra*=229,330)

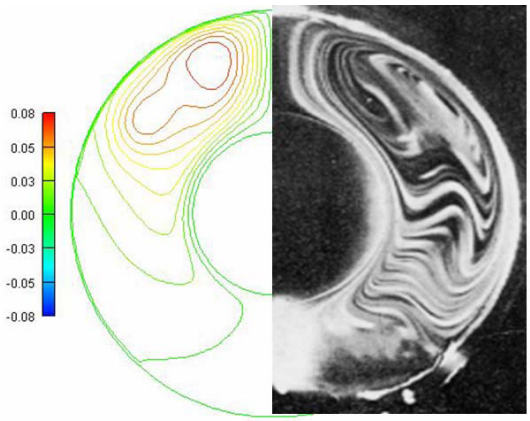

(c) Kidney-shaped eddy flow (*Di*/*d*=1.3, *Ra*=749,760)

Fig. 2. Comparison of the results of the numerical streamlines and Yin's experiment.

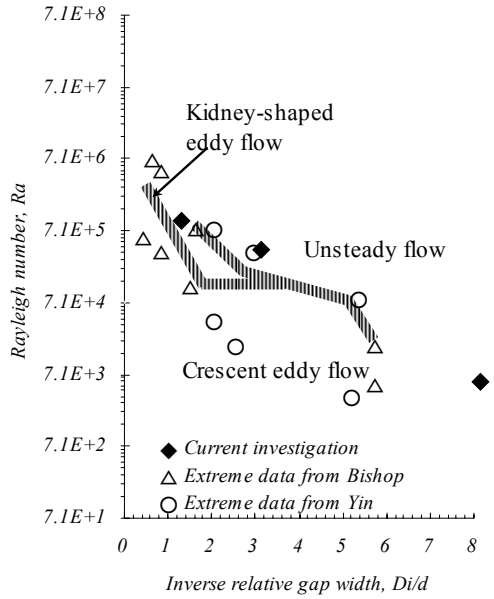

Fig. 3. Categorization of flow regimes for air.

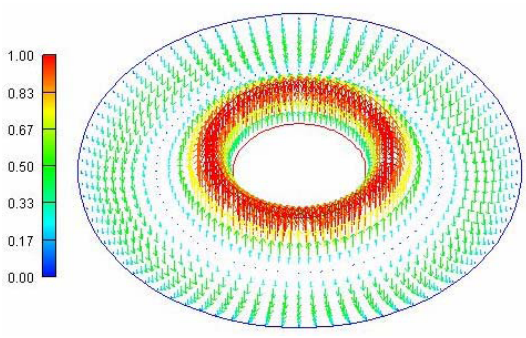

(a) Velocity vectors at θ=90°

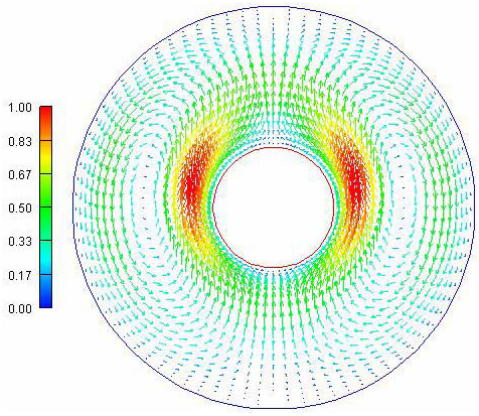

(b) Velocity vectors at ϕ=90°

Fig. 4. Velocity vector (Pr=0.025, Ra=100, and t=100).

magnetic fields. The time for applying the magnetic field was determined as a manner of dimensionless time, t=12. The flow in this time shows a steady state due to the fully developed flow. Here, a modified B method is required to analyze electromagnetic fields in order to investigate the induced electromagnetic field for such flows. In addition, a Φ method is required to calculate the flow at the same condition. The conditions used in this calculation were determined as Pr=0.025, Ra=100, Ta=0, Ha=100 (the Φ and B methods), and Rem=1 (the B method). Fig. 5 shows a section of the velocity vector in a spherical coordinate system at θ=90°and ϕ=90°. It shows that the Φ and B methods represent an agreement in their results qualitatively. In non-electromagnetic fields, the fluid velocity developed at around the wall surface of the inner sphere as shown in Fig. 4 and the flow was transferred toward the upper section of the outer sphere. Whereas, the velocity vector showed the largest value at the side of the inner sphere. Also, the flow developed at around the inner sphere could not approach to the upper region of the sphere and moved to the lower region of the sphere. Then, the pattern of the flow generally demonstrated such Kidney-shaped eddy flow. If certain electromagnetic fields are applied to this flow, the fluid velocity will be restrained as shown in Fig. 5. The velocity vector represented in both methods shows a weaken state that almost approaches 0 except for the side region of the inner sphere. This type of convection restraint effect can be mentioned as the results of the application of Lorentz forces. Fig. 6 shows the scale of the velocity vector along the Z direction of the section at θ=90° and ϕ=90°. This data also represents the convection restraint effect. As shown in Fig. 7, however, the temperature field did not demonstrate a certain change in temperature. This is due to the small Ha number applied in the calculation. In general, it is not possible to ignore Joule heats when the applied Ha number is large.

Meanwhile, the magnetic flux density illustrated in Fig. 8 being shown a difference between the Φ method and the B method. The Φ method is processed to velocity fields as a type of constant imposed fields, but the B method represents different values according to applied locations. In Fig. 8, the scale of the magnetic field produced by the B method represents a change in the magnetic field based on the imposed magnetic field of "1" from the inner sphere (r=0.3) through the outer sphere (r=1). In particular,

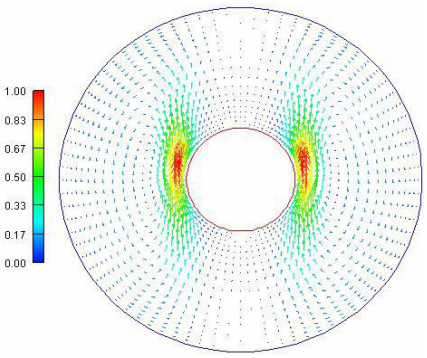

(a) Velocity vectors at ϕ =90° (Φ method)

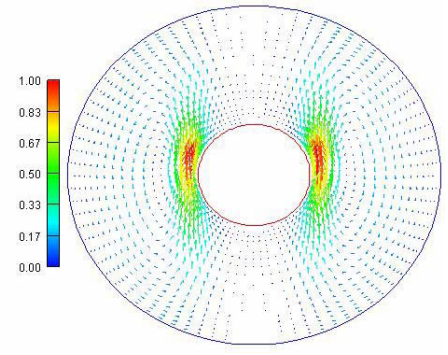

(b) Velocity vectors at ϕ =90° (B method)

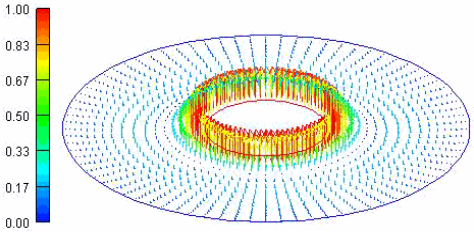

(c) Velocity vectors at θ=90° (B method)

Fig. 5. Velocity vector (Ta=0, Ha=100, Rem=1, t=22).

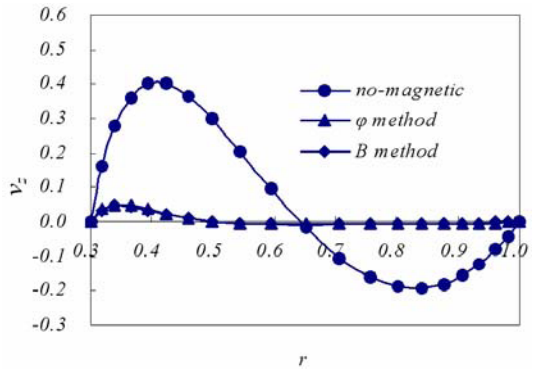

Fig. 6. Velocity profiles at θ=90°, ϕ =90°.

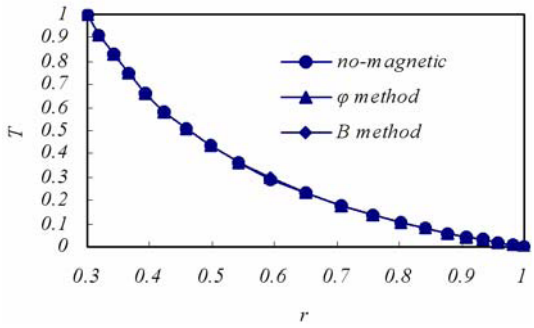

Fig. 7. Temperature profiles at θ=90°, ϕ =90°.

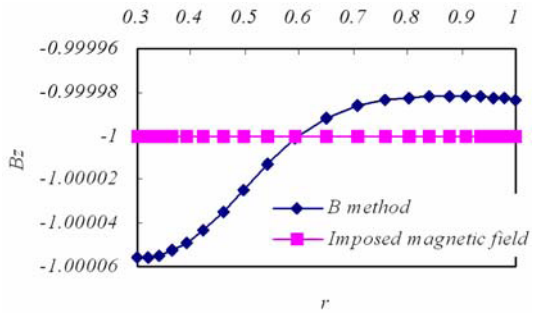

Fig. 8. Magnetic flux density profiles at θ=90°, ϕ =90°.

the magnetic field flow field represents larger values than 1, and the location that shows the same direction represents smaller values than 1. Here, the magnetic field that represents larger values than 1 is due to the fact that the induced current produces new magnetic fields around the surrounding. It causes that the induced current to significantly enforce the imposed magnetic field and that is called as a dynamo operation. However, it shows too small values to affect the flow field. Thus, the results of the velocity and temperature in both the Φ and B method demonstrate the same values. However, it is expected that if the Ra and Rem number applied to the calculation are determined as large values, the results will be varied. It requires further studies.

4.3 Convection of the mercury in Coriolis force fields

This section considers the convection of molten metals in Coriolis force fields. The Coriolis force can occur by the object that shows relative motion in a rotational coordinate system in which the Coriolis

force is normally applied to the direction of relative motion and rotational axis. Thus, it demonstrates a stable state in its flow because the Coriolis force affects the vector component of the direction of the rotational axis for a normal direction. In addition, it is known that the vector component that is normally applied to the rotational axis causes the secondary flow inside the surface due to the applied Coriolis force.

Next, the results of the calculation by using a concentric sphere model can be described as follows. The dimensionless conditions for the calculation for Ra=100 were determined as Ta=10^2, Ta=10^3, and Ta=10^4. Also, the calculation was continued until the time that shows a stable moment in the thermal convection caused by the Coriolis force. Fig. 9 shows the results of the calculation for Ta=10^4. Fig. 9(a) demonstrates the velocity vector of the horizontal surface at θ=90°. As shown in Fig. 9, the effects of the applied Coriolis force at the center of the sphere can be clearly observed. Also, there are strong upward flows with a boundary layer in the surface of the inner sphere. The upward flows were changed and flowed as downward flows at the surface of the outer sphere. The velocity vector illustrated in Fig. 9(a) represents a difference in the direction of the upward flows compared to that of the flow where the Coriolis force was not applied. The velocity vector along the rotational axis was sloped to the west due to the interaction with the Coriolis force. It can be considered that the scale and direction of this vector will be varied according to the scale of the Coriolis force. Although the velocity vector shown in Fig. 9(b) demonstrates a large difference in flow speeds compared to that of the velocity vector represented in Fig. 9(b), there are no significant differences in the direction of the flow velocity. Also, it shows no differences in the Kidney-shaped convection pattern formed on the left and right side of the inner sphere. As a result, it is evident that the calculation conditions of Ta=0 and Ta=10^4 did not affect the pattern variation of the flow.

Fig. 10(a) shows the distribution of the flow velocity ($-v_\phi$) for the horizontal section at θ=90° and ϕ =90°. The nodes determined from r=0.3 to r=1 were used to extract the velocity vector of the r direction.

In addition, it shows that the results of the analysis were applied at the time (t=40) that showed the fully developed velocity. For Ta=0 as shown in Fig. 10, the velocity ($-v_\phi$) was close to 0 for the r direction because the Coriolis force was not applied. However, if the condition was configured as Ta=100, it shows a significant difference in the velocity distribution. First, the velocity ($-v_\phi$) represents an increase in the region defined from r=0.3 to r=0.76. However, there are no significant changes in other regions. Thus, it shows that the change in the flow occurs at around the inner sphere in which the location determined as r=0.5 shows the largest influence of the Coriolis force. Although the scale of the term of $-v_\phi$ that is only applied to the r direction represents a small value, which is determined as 1/10 of the v_z, the influence of the Coriolis force is large. Therefore, the terms of $-v_\phi$ and v_r can be largely affected and moved. It is expected that this flow mechanism can be used in certain fields where different types of fluid are mixed. Next, the results of the calculation for Ta=10^3 and Ta=10^4 show the same aspect as the calculation for Ta=10^2. Also, it can be seen that the increment rate of the maximum flow velocity, $-v_\phi$, decreased for Ta=10^4. In addition, the decrement rate of the flow velocity decreased at r=0.88. There are some reports that such changes in the flow also depend on the scale of the inner sphere.

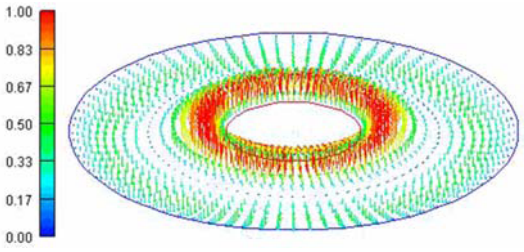

(a) Velocity vectors at θ=90°

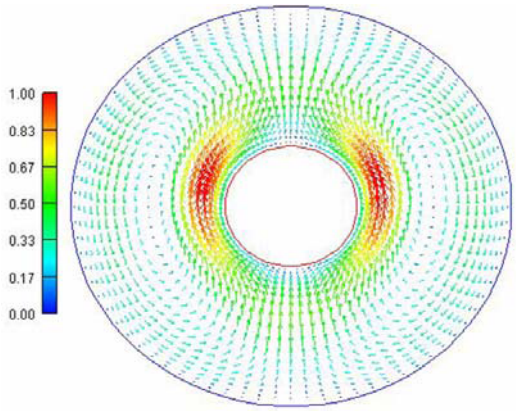

(b) Velocity vectors at ϕ =90°

Fig. 9. Results at t=40 (Ta=10^4, Ha=0, Rem=0).

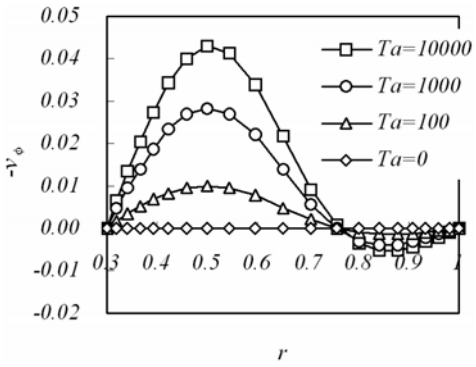

(a) Velocity component $-v_\phi$ at the radius direction

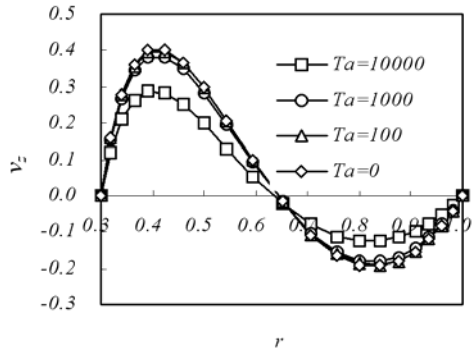

(b) Velocity component v_z at the radius direction.

Fig. 10. Velocity profiles at θ=90°, ϕ=90° (*Ha*=0, *Rem*=0, *t*=40).

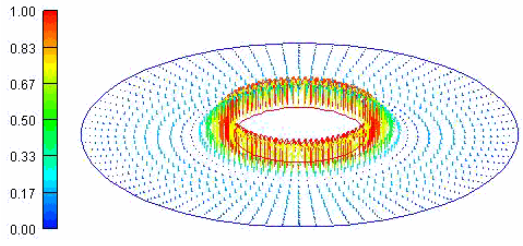

Fig. 11. Results at *t*=40 (θ=90°, *Ta*=10^4, *Ha*=100, *Rem*=1).

Fig. 10(b) shows the distribution of v_z of the section at θ=90˚ and ϕ=90˚. It shows the quantitative values of the upward and downward flow represented in Fig. 9(b). Whereas, the upward flow was observed at the range determined from *r*=0.3 to *r*=0.65, and the downward flow was shown at the range determined from *r*=0.65 to *r*=1. Also, it can be seen that the Coriolis force affected the upward and downward flow as presented in Fig. 10(b). Regarding the condition for *Ta*=10^2 and *Ta*=10^3, there are no significant changes in the flow velocity. However, for *Ta*=10^4, the term of

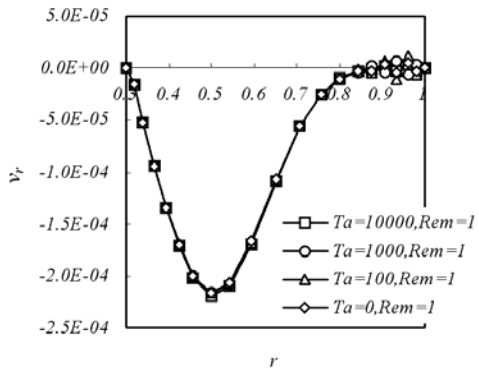

(a) Velocity component v_r at the radius direction

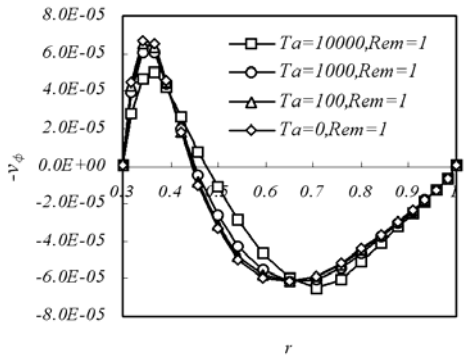

(b) Velocity component $-v_\phi$ at the radius direction

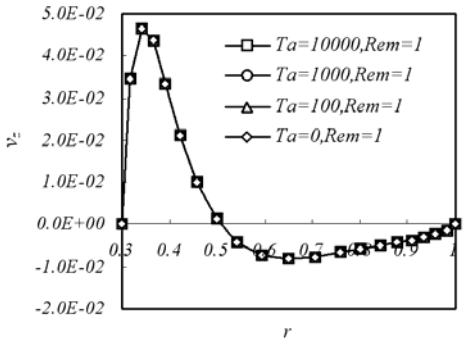

(c) Velocity component v_z at the radius direction.

Fig. 12. Velocity profiles at θ=90°, ϕ=90° (*Ha*=100, *Rem*=1, *t*=40).

v_z shows a large decrease in its values due to the large effect of such a condition. This is due to the fact that the Coriolis force applied to the plane at θ=90˚ attracts the velocity vector component, which is applied along the axial direction. Thus, the velocity vector around the inner sphere illustrated in Fig. 9(a) towards a reverse direction for the rotational axis. In particular, in the calculation for *Ta*=10^4, almost con-

vection components along the axial direction are restrained. It is the characteristics of the flow field that is influenced by the Coriolis force.

4.4 Convection of the mercury with Coriolis and Lorentz forces

This section considers the natural convection of the molten metal where electromagnetic fields and Coriolis forces are applied at the same time. From the results of the analysis of this case, it is evident that the Coriolis force affected such thermal convection. Fig. 11 shows the results of the application of the Coriolis force for the velocity field where magnetic files are applied as illustrated in Fig. 5(c). The former represents a large change in the velocity vector around the inner sphere compared to that of the latter. It was due to the fact that the velocity vector with magnetic fields along the axial direction was influenced by the additional Coriolis force. Thus, it is clear that the convection can be strongly restrained. Also, it can be verified by the velocity distribution illustrated in Fig. 12. From the velocity distribution as shown in Fig. 12(b), the flow velocity was restrained at a section determined from r=0.3 to r=0.65. The restraint effect represents the largest level for Ta=10^4. However, the flow velocity, v_r, shown in Fig. 12(a) was not influenced by the scale of the applied Ta number. Also, the flow velocity, v_z, shown in Fig. 12(c) was not influenced by the Ta number. These are the characteristics of the flow field applied by the Lorentz and Coriolis force.

5. Conclusions

This study performed numerical analyses for two different working fluids. One was an analysis of natural convection with air that was compared with the results of applied experiments. The other was an investigation for the relationship between velocity field, electromagnetic field, and temperature field in a model with molten metal. Whereas, the influences of the Coriolis force on the flow field were investigated. The results can be summarized as follows:

From the results of the calculation for Ra=5,964, Ra=229,330, and Ra=749,760, it showed excellent agreement with the visualization test done by Yin. In the experiment, the vortex represented an unsteady state, and the calculation showed a steady state. Thus, it was possible to simulate the vortex shape through the steady calculation.

In order to investigate the role of induced magnetic field, the modified B method was used to analyze such electromagnetic fields. From the analysis of flow fields, the B and Φ method represented an agreement between these results. However, the B method showed better electromagnetic characteristics than the Φ method for the same conditions (Pr=0.025, Ra=100, Ta=0, Ha=100 (both the Φ and B method), and Rem=1 (the B method).

The dynamo operation which the induced magnetic field strengthened the imposed magnetic field was investigated by the modified B method. The Φ method was processed to flow fields by using a constant scale of magnetic fields (x, y, z=0, 0, -1), and the B method showed differences in magnetic fields according to the applied location. The section where the direction of the imposed magnetic field and the reversed flow occurred at θ=90˚ and Φ =90˚ showed larger magnetic fields than 1. Also, the section where the forward flow occurred for the imposed field showed smaller values than 1.

Under the condition where were no magnetic fields, it was evident that the Coriolis force had two effects on the flow field. One was that the velocity vector of the rotational axis was sloped to the west at θ=90˚. The other was that the velocity component, which is normally applied to the rotational axis, showed an increase in the flow velocity at Φ =90˚ locally.

The interaction between the magnetic field and the Coriolis force showed a significant level at θ=90˚. Also, the flow around the inner sphere that included the velocity component along the rotational axis largely affected by the Lorentz force according to the increase in the Ta number. It means that the results improved the convection restraint effect.

Nomenclature

B	:	Dimensionless magnetic flux density vector
C_p	:	Specific heat at constant pressure
Di	:	Diameter of inner sphere
d	:	Gap width between spheres=r_o-r_i
Ec	:	Eckert number
Ek	:	Ekman number
$\hat{g}$	:	Unit vector of gravity direction
g	:	Gravitational acceleration
H	:	Dimensionless Bernoulli function=p+v^2/2
Ha	:	Hartmann number
j	:	Dimensionless current density vector

k : Unit vector along the rotational axis
Pe : Peclet number=$Re \cdot Pr$=1
Pr : Prandtl number
R : Dimensionless cross helicity= $(\nabla \cdot B)/Rem$
Ra : Rayleigh number=$Gr \cdot Pr$
Rem : Magnetic Reynolds number=Ud/ν_m
r : Radial coordinate
r_i : Radius of inner sphere
r_o : Radius of outer sphere
T : Dimensionless temperature
Ta : Taylor number
t : Dimensionless time
U : Representative velocity
v : Dimensionless velocity vector

Greek symbols

Φ : Electric scalar potential
α : Thermal diffusivity
β : Thermal expansion coefficient
ΔT : Temperature difference between spheres
θ : Angular coordinate measured positive clockwise
ν : Kinematic viscosity
ν_m : Magnetic viscosity=1/ ($\sigma\mu$)
ρ : Fluid density
σ : Electric conductivity
ϕ : Azimuthal angle
ω : Dimensionless vorticity vector=$\nabla \times v$
Ω : Angular velocity

Subscripts

i : Inner wall
o : Outer wall

References

[1] A. Kageyama, T. Sato, K. Watanabe, R. Horiuchi, T. Hayashi, Y. Todo, T. H. Watanabe and H. Takamaru, Computer Simulation of a Magnetohydrodynamic Dynamo. II, *Phys. Plasmas,* 2 (5) (1995) 1421-1431.

[2] Y. Honkura, T. Iijima and M. Matsushima, Magnetic Field Reversal Resulting from a Dynamo Process in a Spherical Shell, *J. Geomag. Geoelectr.,* 44 (1992) 931-941.

[3] G. A. Glatzmaier and P. H. Roberts, A Three-Dimensional Self-Consistent Computer Simulation of a Geomagnetic Field Reversal, *Nature,* 377 September (21) (1995) 203-209.

[4] S. H. Yin, R. E. Powe, J. A. Scanlan and E. H. Bishop, Natural Convection Flow Patterns in Spherical Annuli, *Int. J. Heat Mass Transfer,* 16 (1973) 1785-1795.

[5] E. H. Bishop, L. R. Mack and J. A. Scanlan, Heat Transfer by Natural Convection between Concentric Spheres, *Int. J. Heat Mass Transfer,* 9 (1996) 649-662.

[6] H. S. Chu and T. S. Lee, Transient Natural Convection Heat Transfer between Concentric Spheres, *Int. J. Heat Mass Transfer,* 36 (13) (1993) 3159-3170.

[7] V. K. Garg, Natural Convection between Concentric Spheres, *Int. J. Heat Mass Transfer,* 35 (8) (1992) 1935-1945.

[8] C. P. Chiu and W. R. Chen, Transient Natural Convection Heat Transfer between Concentric and Vertically Eccentric Spheres, *Int. J. Heat Mass Transfer,* 39 (7) (1996) 1439-1452.

[9] S. Y. Yanase, J. Mizushima and K. Araki, Multiple Solutions for a Flow between Two Concentric Spheres with Different Temperatures and Their Stability, *J. Phys. Soc. Japan,* 64 (7) (1995) 2433-2443.

[10] Y. Kato and T. Tanahashi, Finite-Element Method for Three-Dimensional Incompressible Viscous Flow Using Simultaneous Relaxation of Velocity and Bernoulli Function, *JSME Int. J.,* Series II 35 (3) (1992) 346-353.

[11] T. Tanahashi, Y. Oki and K. Henjes, An Application of GSMAC-FEM to Electrically Conducting Fluid Flows Driven by Lorentz Force, *Comp. Fluid Dyn.,* 1 (1993) 233-248.

[12] Y. Oki and T. Tanahashi, Entrance Flows of Electrically Conducting Fluids between Two Parallel Plates, *JSME Int. J.,* Series B 37 (2) (1994) 328-335.

[13] C. H. Jung, Y. Ogawa and T. Tanahashi, Numerical Simulation of MHD Fluids Using GSMAC-FEM in Two Concentric Spheres, *Proc. 4th KSME-JSME Fluids Eng. Conf.*, Haeundae, Pusan, Korea. (1998) 609-612.

[14] C. H. Jung and T. Tanahashi, GSMAC-FEM Analysis of Single-Crystal Growth by Cusp MCZ Method, *KSME Int. J.,* 15 (12) (2001) 1876-1881.

[15] C. H. Jung, T. Minowa and T. Tanahashi, Numerical Analysis on Molten Metal under Magnetic Field Using GSMAC-FEM Method, *Pro. 4th JSME-KSME Thermal Eng. Con.*, Kobe, Japan. (2000) 529-536.

[16] C. H. Jung, T. Minowa and T. Tanahashi, Numerical Analysis of Molten Metal under Magnetic Field Using ALE Method, *JSME Int. J.,* Series A 45 (2) (2002) 153-160.